

# LA-UR-13-23383

Approved for public release; distribution is unlimited.

Title: Experimental Investigations -- Midyear Status Report

Author(s): Ulrich, Timothy J. II  
Anderson, Brian E.  
Le Bas, Pierre-Yves  
Tokash, Justin C.  
Riviere, Jacques V.  
Ohara, Yoshikazu  
Haupt, Sylvain

Intended for: Report

Issued: 2013-05-09



**Disclaimer:**

Los Alamos National Laboratory, an affirmative action/equal opportunity employer, is operated by the Los Alamos National Security, LLC for the National Nuclear Security Administration of the U.S. Department of Energy under contract DE-AC52-06NA25396. By approving this article, the publisher recognizes that the U.S. Government retains nonexclusive, royalty-free license to publish or reproduce the published form of this contribution, or to allow others to do so, for U.S. Government purposes. Los Alamos National Laboratory requests that the publisher identify this article as work performed under the auspices of the U.S. Department of Energy. Los Alamos National Laboratory strongly supports academic freedom and a researcher's right to publish; as an institution, however, the Laboratory does not endorse the viewpoint of a publication or guarantee its technical correctness.

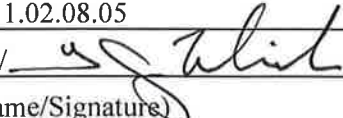
# FCT Quality Assurance Program Document

## Appendix E FCT Document Cover Sheet

Name/Title of Deliverable/Milestone M3FT-13LA0805031 / Experimental Investigations  
– Midyear Status Report / M3

Work Package Title and Number ST Storage and Transportation Experiments –  
LANL. FT-13LA080503

Work Package WBS Number 1.02.08.05

Responsible Work Package Manager Timothy J. Ulrich II /   
(Name/Signature)

Date Submitted \_\_\_\_\_

Quality Rigor Level for Deliverable/Milestone  QRL-3  QRL-2  QRL-1  N/A\*  
 Nuclear Data

This deliverable was prepared in accordance with Los Alamos National Laboratory  
(Participant/National Laboratory Name)

QA program which meets the requirements of  
 DOE Order 414.1  NQA-1-2000  Other

**This Deliverable was subjected to:**

Technical Review

**Technical Review (TR)**

**Review Documentation Provided**

- Signed TR Report or,
- Signed TR Concurrence Sheet or,
- Signature of TR Reviewer(s) below

**Name and Signature of Reviewers**

James A. TenCate (DC)  
\_\_\_\_\_  
\_\_\_\_\_  
\_\_\_\_\_

Peer Review

**Peer Review (PR)**

**Review Documentation Provided**

- Signed PR Report or,
- Signed PR Concurrence Sheet or,
- Signature of PR Reviewer(s) below

  
\_\_\_\_\_  
\_\_\_\_\_  
\_\_\_\_\_

*\*NOTE In some cases there may be a milestone where an item is being fabricated, maintenance is being performed on a facility, or a document is being issued through a formal document control process where it specifically calls out a formal review of the document. In these cases, documentation (e.g., inspection report, maintenance request, work planning package documentation or the documented review of the issued document through the document control process) of the completion of the activity along with the Document Cover Sheet is sufficient to demonstrate achieving the milestone. QRL for such milestones may also be marked N/A*

# ***Experimental Investigations -- Midyear Status Report***

**Fuel Cycle Research & Development**

*Prepared for  
U.S. Department of Energy  
Used Fuel Campaign  
T.J. Ulrich, B.E. Anderson, P.-Y. Le  
Bas, J. Riviere, J.C. Tokash, S.  
Hauptert, C. Payan and Y. Ohara  
Los Alamos National Laboratory  
15 April 2013  
FCRD-NFST-2013-000156*



#### **DISCLAIMER**

This information was prepared as an account of work sponsored by an agency of the U.S. Government. Neither the U.S. Government nor any agency thereof, nor any of their employees, makes any warranty, expressed or implied, or assumes any legal liability or responsibility for the accuracy, completeness, or usefulness, of any information, apparatus, product, or process disclosed, or represents that its use would not infringe privately owned rights. References herein to any specific commercial product, process, or service by trade name, trade mark, manufacturer, or otherwise, does not necessarily constitute or imply its endorsement, recommendation, or favoring by the U.S. Government or any agency thereof. The views and opinions of authors expressed herein do not necessarily state or reflect those of the U.S. Government or any agency thereof.



## **SUMMARY**

This report summarizes technical work conducted by LANL staff and international collaborators in support of the UFD Storage Experimentation effort. The current focus of this technical work is two-fold: 1) on the stainless steel (304L) failure mechanism known as stress corrosion cracking (SCC), and 2) on the concrete integrity under degradation conditions (e.g., thermal, radiation, alkali-aggregate reactions). As these issues are common among our international partners, a significant effort has been put forth to engage foreign programs in a mutually beneficial collaborative program on these topics. Results from these collaborations, notably with Japan, France and Switzerland, are highlighted.

## CONTENTS

SUMMARY .....	iv
ACRONYMS .....	viii
1. INTRODUCTION .....	1
2. SCC Sample preparation.....	1
2.1 SCC Detection and Imaging.....	3
3. Concrete Integrity Research .....	9
3.1 EvaDéOs Project Summary.....	9
3.2 Scope of Work.....	9
3.2.1 Blocks .....	10
3.2.2 Wall.....	11
3.3 EvaDéOs Results.....	13
3.4 Additional Concrete Studies.....	13
4. References.....	14
Proceedings Paper Prepared for the 2013 Spring Meeting of the Acoustical Society of America, Montreal Canada.....	15
Manuscript In Preparation for Peer Review.....	19

## FIGURES

Figure 1: Stress corrosion cracking damage of a Type 304 stainless steel U-Bend sample. Test conditions: $T = 95^{\circ}\text{C}$ , aqueous 42 wt% magnesium chloride solution, time to failure was 89 hours. ....	2
Figure 2: Type 304L stainless steel welded disk for SCC damage tests.....	2
Figure 3: Type 304L circularly welded plate for SCC damage testing. ....	2
Figure 4: Experimental apparatus for SCC formation. ....	3
Figure 5: Imaging results of the SCC specimen using SPACE. ....	4
Figure 6: Photos of the sliced SCC specimen. Sample 6a shown in close up of the crack tip. ....	5
Figure 7: Experimental setup for NRUS and modal imaging.....	5
Figure 8: Resonance spectrum of sliced SCC sample.....	6
Figure 9: Vibrational modes of the SCC sample. ....	7
Figure 10: Resonance spectra obtained from NRUS measurements in the ranges of (a) 4 – 4.5 kHz and (b) 12 - 12.5 kHz. ....	7
Figure 11: Nonlinear peak shift as a function of drive amplitude. ....	7
Figure 12: Frequency responses averaged over the specimen due to single frequency excitations at (a) 4.28 kHz and (b) 12.33 kHz. ....	8

Figure 13: Location of measurement points on concrete blocks. .... 10  
Figure 14: Concrete wall with carbonation zones identified. .... 11  
Figure 15: Location of measurement points on the concrete wall. .... 12

**TABLES**

Table 1: Concrete block distribution..... 10  
Table 2: Summary of measurements to be made on concrete blocks..... 11  
Table 3: Summary of measurements to be made on concrete wall..... 13



## ACRONYMS

AAR	Alkali Aggregate Reaction
ANR	National Research Agency (France)
ASTM	American Society for Testing and Materials
DAE(T)	Dynamic Acousto-Elasticity (Technique)
EES-17	Geophysics Group at LANL
EMPA	Eidgenössische Materialprüfungs- und Forschungsanstalt (Swiss Federal Laboratory for Materials Science and Technology)
ETH	Eidgenössische Technische Hochschule (Swiss Federal Institute of Technology, Zurich)
FCT	Fuel Cycle Technologies
GPR	Ground Penetrating Radar
LANL	Los Alamos National Laboratory
LANSCE	Los Alamos Neutron Science Center
LCND	Laboratoire de Caractérisation Non Destructive (Nondestructive Characterization Laboratory, Aix-en -Provence, France), now part of the LMA
LMA	Laboratoire de Mécanique et d'Acoustique (Laboratory of Mechanics and Acoustics, Marseille, France)
MST-6	Metallurgy Group at LANL
NEWS	Nonlinear Elastic Wave Spectroscopy
NLUT	Nonlinear Ultrasonic Techniques
NRUS	Nonlinear Resonant Ultrasound Spectroscopy
QAPD	Quality Assurance Program Document
RUS	Resonant Ultrasound Spectroscopy
SCC	Stress Corrosion Cracking
SPACE	Sub-harmonic Phased Array for Crack Evaluation
TREND	Time Reversal Elastic Nonlinearity Diagnostic





# USED FUEL DISPOSITION CAMPAIGN / STORAGE & TRANSPORTATION EXPERIMENTS PROGRAM

## 1. INTRODUCTION

This document describes the technical work dealing with the determination of the potential for nonlinear elastic wave spectroscopy (NEWS) and other nonlinear ultrasonic techniques (NLUT) to be used for detection, monitoring, characterization and imaging of material degradation in materials relevant to the storage of used nuclear fuel. Particular importance has been placed upon stress corrosion cracking of stainless steel (304L) and various degradation mechanism of concrete due to the ubiquity of these materials in nuclear fuel storage facilities. This work was carried out at the Los Alamos National Laboratory in accordance with the Fuel Cycle Technologies (FCT) Quality Assurance Program Document (QAPD).

## 2. SCC Sample preparation

Austenitic stainless steels are known to be susceptible to stress corrosion cracking (SCC), which is an aggressive type of corrosion that exists when a material under tensile stress is placed in a corrosive environment. This is of particular concern because weld joints produce an inherent residual stress in metals that can lead to SCC, therefore our goal is to study the formation of stress corrosion cracks within Type 304L stainless steel, which is frequently used in containers for used nuclear fuel disposal. The work within MST-6 at LANL is to produce damaged stainless steel samples that can be used within EES-17 to develop and test nondestructive nonlinear acoustic techniques and apply them to detect the onset of SCC.

In order to determine the appropriate conditions to induce SCC, the first set of experiments were conducted on U-Bend samples. The U-Bends are simply a thin strip of Type 304 stainless steel (1/16" thick) that are bent around a 1" diameter rod such that the final form is in a U shape. These samples result in tensile stress along the outer surface of the bend and compressive stress on the inner surface. The U-Bends are held in their final stressed state with the aid of a bolt along the top edge of the straight arms, otherwise they deflect by approximately 60 degrees in the un-sprung state.

One of the most aggressive initiators of SCC is the chloride anion; therefore, the U-Bends samples were tested in hydrochloric acid, hydrochloric acid plus sodium chloride, and magnesium chloride solutions. It is known that SCC is temperature dependent, so the U-Bends samples were tested at various temperatures from 30-95°C. The best results (i.e., through cracking in less than 5-days) were obtained at 95°C in a 42 wt% solution of magnesium chloride (Figure 1).

Because the goal of this work is to study materials that would be used for the storage or disposal of spent nuclear fuel, the next step will be to induce stress corrosion cracks on welded Type 304L stainless steel samples. The first of the welded samples is a V-welded split-disk that is 8" in diameter and 3/4" thick (Figure 2). The residual stress in this welded disk is clearly present due to the high degree of warping observed in the sample. The second welded sample is a circular weld on a 4" x 4" square plate, which caused residual stress that can be seen in Figure 3 where the plate has gone from a flat piece to slightly bowl-shaped. Based on the U-Bend samples, the welded samples will be damaged in 42 wt% magnesium chloride at 95°C and delivered to EES-17 for acoustic testing.

In the remainder of FY13, the LANL prepared samples will be tested using various NEWS techniques to determine the most appropriate method(s) to use for monitoring SCC development. The testing this year will focus on defining measurement sensitivity at the condition bounds (i.e., undamaged and critically damaged) in preparation for the continual monitoring to begin in FY14.



Figure 1: Stress corrosion cracking damage of a Type 304 stainless steel U-Bend sample. Test conditions: T = 95°C, aqueous 42 wt% magnesium chloride solution, time to failure was 89 hours.



Figure 2: Type 304L stainless steel welded disk for SCC damage tests.

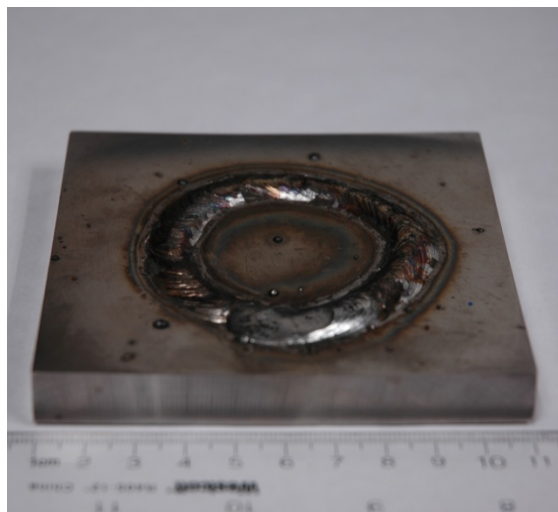


Figure 3: Type 304L circularly welded plate for SCC damage testing.

## 2.1 SCC Detection and Imaging

Dr. Yoshikazu Ohara visited LANL for 3 weeks in March of this year. Dr. Ohara is an Engineering Professor from Tohoku University in Sendai, Japan, where his research focuses on nondestructive testing using linear and nonlinear ultrasound for the inspection of industrial parts, among them nuclear reactor components. One important failure mechanism of concern in nuclear reactor materials is SCC, specifically of 304L stainless steel. Though the components may differ, this failure mechanism and material are common concerns for UFD Storage applications. In order to initiate a longterm collaboration on this topic, for the mutual benefit of both the USA and Japanese governments, Dr. Ohara was invited to conduct nonlinear ultrasound testing on samples prepared and inspected in Japan using LANL technologies and facilities.

The samples provided were of sensitized 304L stainless steel containing SCC. The SCC was extended from the tip of a fatigue crack in a solution of 30 wt %  $\text{MgCl}_2$  at 90 °C by using the apparatus shown in Fig. 4. The formation method is described in detail in the Ref. [1]. Before visiting, Dr. Ohara measured the SCC specimen using a nonlinear ultrasonic imaging apparatus, which he developed. This technique/apparatus is termed Sub-harmonic Phased Array for Crack Evaluation (SPACE)[2,3], based on the subharmonic waves generated by large-amplitude short burst and phased array algorithm with frequency filtering. In SPACE, open and closed cracks can be imaged in fundamental and subharmonic images, respectively. As shown in Fig. 5, the SCC was readily observed in the subharmonic image. This indicates that the SCC is closed, as the mechanism for subharmonic generation is a *clapping* mode, i.e., motion referred to as mode I in traditional fracture mechanics.

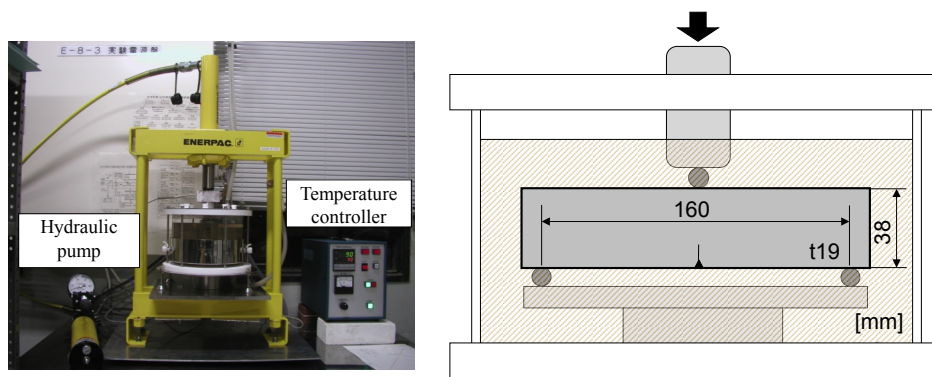


Figure 4: Experimental apparatus for SCC formation.

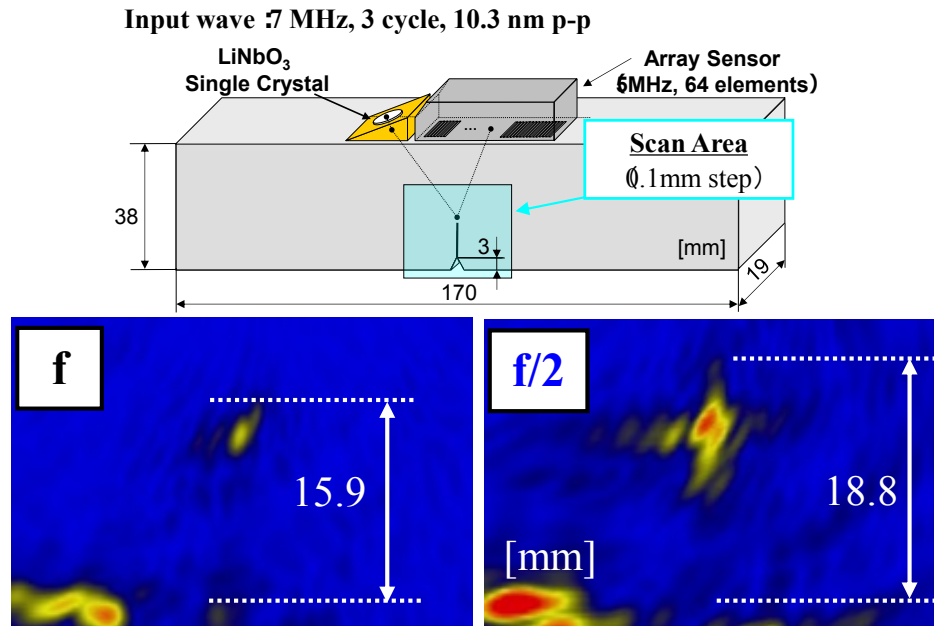


Figure 5: Imaging results of the SCC specimen using SPACE.

Dr. Ohara worked with LANL scientists to conduct nonlinear resonant ultrasound spectroscopy (NRUS) measurements, specifically by focusing on the multi-mode nonlinear resonance ultrasound spectroscopy. Multi-mode NRUS is able to locate nonlinear local defects by utilizing the change in sensitivity to the defects depending on the resonant mode.[4] Prior studies have purported the usefulness of Multi-mode NRUS as verified in numerical simulations, however, the experimental verification had yet to be reported. The objective of this NRUS measurement is to verify the capabilities of Multi-mode NRUS for defect detection and location through experimental observation and testing.

For this measurement the sliced specimen, shown in Fig. 6, was used. The photos of the experimental setup are shown in Fig. 7. The specimen was excited with a PZT disc (10 mm in diameter and 2 mm in thickness). The vibration was measured with a scanning laser vibrometer (Polytec PSV-400). The NRUS measurement was performed using RITA<sup>®</sup> (Resonant Inspection Techniques & Analyses) software developed at LANL.

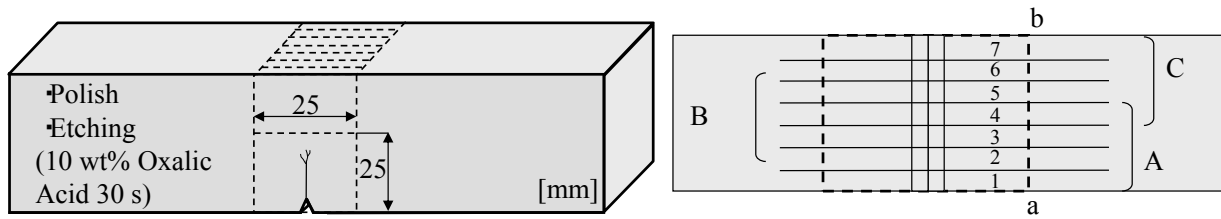


Figure 6: Photos of the sliced SCC specimen. Sample 6a shown in close up of the crack tip.

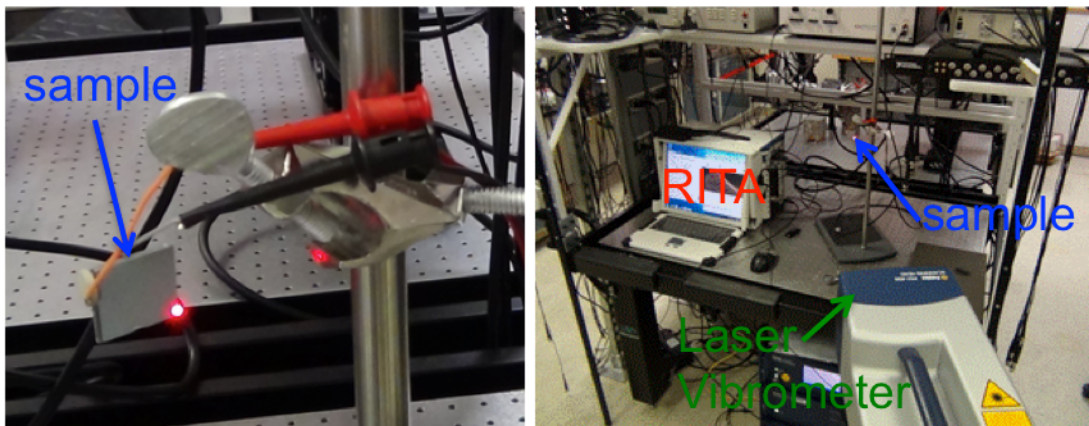


Figure 7: Experimental setup for NRUS and modal imaging.

The resonance spectrum of the measured specimen is shown in Fig. 8. To experimentally validate Multi-mode NRUS, detailed measurements and analysis were made for resonance peaks at 4.28 kHz and 12.33 kHz. These peaks were selected from the spectrum due to their modal shapes. The vibration pattern, i.e., modal shape, for each of these frequencies was measured using the scanning laser vibrometer. In Fig. 9(a) the pattern shown corresponds to fundamental resonance mode at 4.28 kHz. Note that the nodal line, i.e., lack of motion, appeared around the crack. In the vibration pattern of the higher mode at 12.33 kHz, the anti-node appeared around the crack, as shown in Fig. 9(b). Thus one would expect NRUS to show a significant shift in the resonance frequency for the 12.33 kHz mode and not for the 4.28 kHz mode. Based on these results, an NRUS measurement was performed for each of the selected modes; data shown in Fig. 10. The excitation voltage was systematically increased from 10 V to 200 V with a step of 10 V for each of the NRUS experiments. Fig. 10(a) shows the dependence of the resonance peak on excitation voltage for the mode at 4.28 kHz. In these spectra no peak shift was observed. Fig. 10(b) shows the dependence of the resonance peak on excitation voltage for frequencies 12 - 12.5 kHz. Contrary to the behavior shown in Fig. 10(a), in this frequency range, a peak shift was clearly visible. Note that the two peaks around 12.3 kHz represent the symmetrical modes due to symmetry in the sample geometry.

To quantify and compare these observations the relative peak shift was plotted against excitation voltage (Fig. 11). Open and closed circles represent the normalized peak shift observed in Figs. 10(a) and 10(b), respectively. The normalized peak shift of Fig. 10(a) was unchanged depending on input voltage, although it fluctuated due to the effect of noise. This suggests, as expected, that the resonant mode shown in Fig. 9(a) is insensitive to the defect. This can be explained due to the fact that the node exists around the crack and therefore the crack is not being activated in this type of motion. In contrast, the normalized peak shift of Fig. 10(b) obviously depended on the input amplitude. This suggests that the vibrational mode of Fig. 9(b) is sensitive to the crack because the anti-node exists around the crack and it causes the nonlinear contact vibration of crack surfaces, including *clapping* and *rubbing*.

To further explore the occurrence of nonlinear contact vibration, the scanning laser vibrometer was used to measure the average frequency response over the specimen due to a single frequency input. At the excitation frequency  $f_f = 4.28$  kHz, the fundamental resonant mode, the presence of  $f_f$  and the higher harmonics of this mode, i.e.,  $2f_f, 3f_f, \dots$  were observed in Fig. 12(a). Due to higher modes having frequencies that can be harmonic of the fundamental mode, it is extremely difficult to separate the harmonic distortion, due to nonlinearity, from the parametric excitation of higher resonance modes. On the other hand, at the excitation frequency  $f = 12.33$  kHz, in addition to the resonance frequency and its harmonics, other spectral components are also present, including modulation of the drive frequency with the fundamental modal frequency[5] (i.e.,  $f \pm f_f$ ), as seen in Fig. 12(b). In contrast to the harmonic frequency amplitudes, these other modulation components provide evidence of the nonlinear contact vibration of the crack.

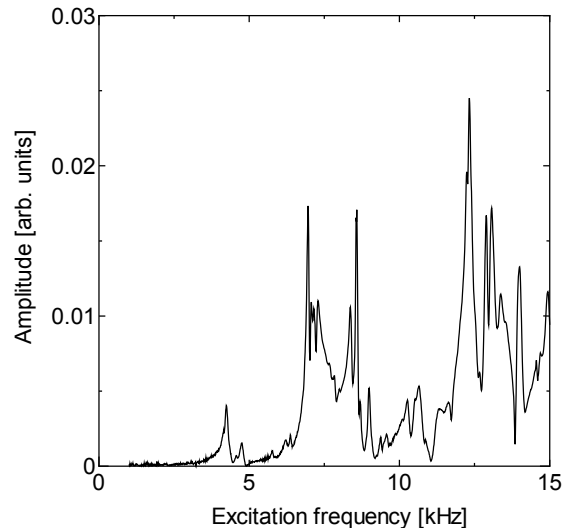
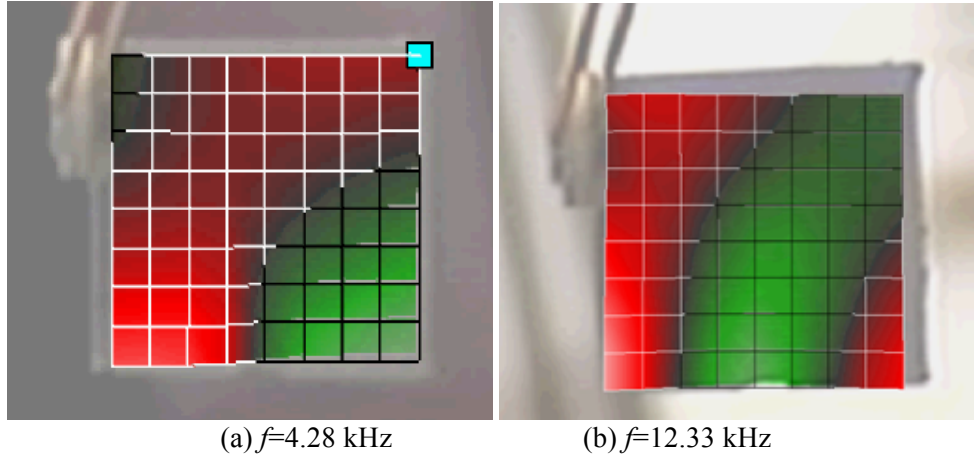


Figure 8: Resonance spectrum of sliced SCC sample.



(a)  $f=4.28$  kHz

(b)  $f=12.33$  kHz

Figure 9: Vibrational modes of the SCC sample. Light red and light green area are anti-node, *i.e.* zones of maximal displacement. The black lines at the transition between those are node of vibration, *i.e.* zone of null displacement.

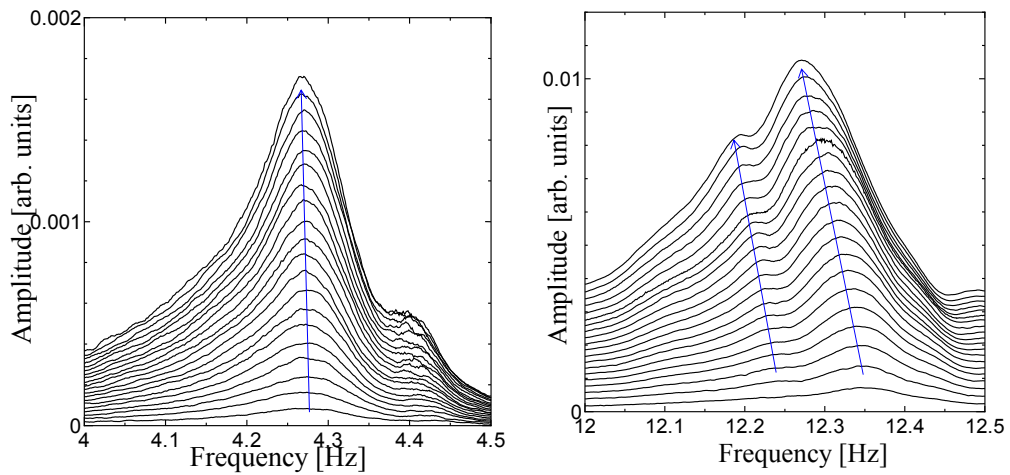


Figure 10: Resonance spectra obtained from NRUS measurements in the ranges of (a) 4 – 4.5 kHz and (b) 12 - 12.5 kHz.

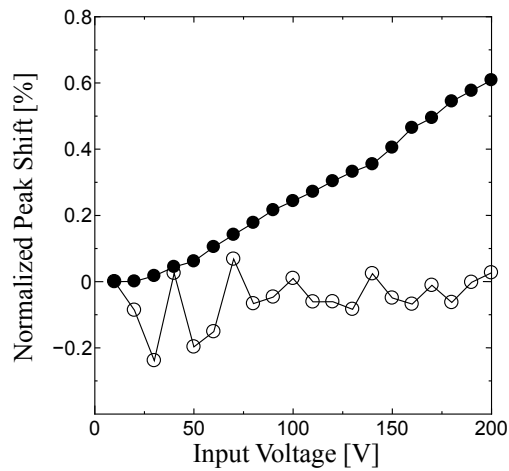


Figure 11: Nonlinear peak shift as a function of drive amplitude. Open circles indicate peak shift from data presented in Fig.10(a); closed circles indicate data from Fig. 10 (b).

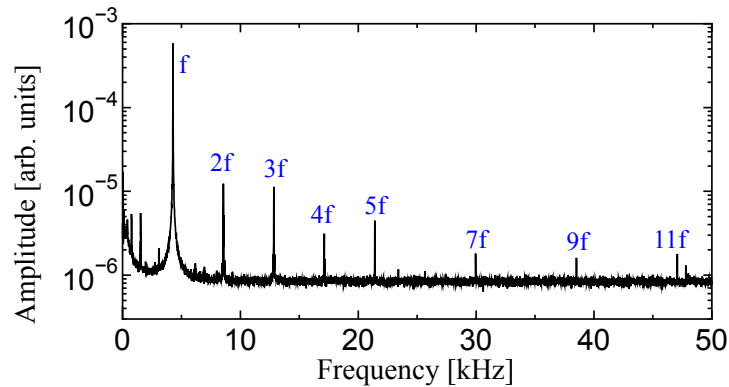
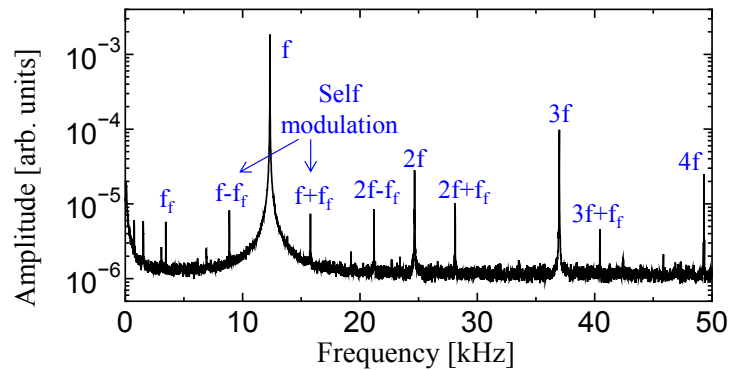
(a) input frequency  $f=4.28$  kHz(b) input frequency  $f=12.33$  kHz

Figure 12: Frequency responses averaged over the specimen due to single frequency excitations at (a) 4.28 kHz and (b) 12.33 kHz.

Other studies of SCC and fatigue cracks were begun during Dr. Ohara's visit, specifically the use of TREND and the Dynamic Acousto-Elasticity Technique (DAET). Analysis for these studies is ongoing and further data will be collected in Aug. 2013 on a return visit of Dr. Ohara to LANL for an additional 3 weeks. Results will be presented in the project end-of-year report. Two additional studies of fatigue cracks appear in Appendices A and B, though no SCC was present in these samples. The studies presented in the appendices are manuscripts in preparation for proceedings and peer-review on general crack orientation determination and observable crack dynamics, both using NLUT.

In addition to the ongoing SCC studies mentioned above, future collaborations with Dr. Ohara will develop an extension of SPACE by using 3D scanning laser vibrometry capabilities at LANL. Dr. Ohara will fabricate a transducer using a Lithium Niobate ( $\text{LiNbO}_3$ ) single crystal, at Tohoku University, to be used as the excitation source for this extended SPACE system. As a receiver LANL's 3D scanning laser vibrometry capabilities will be used in order to simulate a transducer array without the need to disturb the sample with a physical array. The 3D scanning laser vibrometer has a lot of advantages. In addition to its flat broadband frequency characteristics, it is capable of receiving both out-of-plane and in-plane displacements. Furthermore, with an appropriate selection of scanning points it is possible to simulate 2D transducer array with arbitrary element arrangement. This has a potential to produce 3D images of open and closed cracks. Also note that this method is for internal inspection and difficult to use for surface features. The high sensitivity to surface defects, of which LANL's TREND is capable, will be used for detection and imaging near free surfaces. Therefore, the combination of SPACE with TREND would

provide a nonlinear ultrasonic measurement system that is able to inspect both inside and on the surface of structures.

### 3. Concrete Integrity Research

The Agence Nationale de la Recherche (ANR, the French national research agency), is sponsoring a national research effort on the nondestructive evaluation for the prediction of the degradation of structures and the optimization of their monitoring (referred to as EvaDéOs). They are conducting a major experimental campaign during the first half of 2013. LANL was invited to participate by sending a visiting scientist to the French Laboratory of Mechanics and Acoustics (LMA) in Marseille, France. LANL staff scientist Pierre-Yves Le Bas is currently conducting experiments with LMA (Cedric Payan) as part of this collaboration. LANL's invitation and participation are the direct result of the collaborative work conducted with LMA's Cedric Payan at LANL during the Fall of 2011.

#### 3.1 EvaDéOs Project Summary

The following paragraphs are a summary of the EvaDéOs project and its objects (directly translated from the project website in French)[6].

“EvaDéOs The project is part of the research program ‘Sustainable buildings and cities 2011 (BVD 2011)’, funded by the National Research Agency (ANR), which is centered on the sustainability of places of urban life, from the building scale to that of the urban area, in a context of strong and uncertain structural changes.

“This industrial research project aims at integrating a predictive approach with a probabilistic approach to risk analysis of visible degradation in order to develop a comprehensive methodology for monitoring of concrete structures before visible deterioration; incorporating the different phases of building management from the evaluation to the decision making via the diagnosis and prognosis of the damage. Engineered structures and buildings associated with the production of electrical energy are the main structures involved. Since reinforcement corrosion remains the major concern for reinforced concrete structures, the EvaDéOS project is limited only to this problem. The originality of this project is that it fits into a preventive approach (where the damage is not proven but where the necessary conditions are present and thus damage will occurs at shorter or longer term). To achieve this, models of corrosion initiation to predict the penetration of aggressive agents leading to depassivation of rebar are first selected and developed. In a second phase models of corrosion propagation are studied to predict the kinetics of development of the corrosion. The challenge is to obtain degradation indexes to determine the optimal milestones in decision making (economic gain of inspection operations and maintenance), based on the probabilistic forecasted degradations, costs and updates of the current state. Scientists project partners are the following laboratories: the Laboratory of Non Destructive Characterization (LCND, now part of the Laboratory of Mechanics and Acoustics, LMA), the Laboratory of Materials and Durability of Constructions (LMDC), the Institute of Mechanics and Engineering of Bordeaux and the Research Institute of Civil Engineering and Mechanics (GEM) each participating jointly or not to the various themes of the project; namely : estimation of uncertainties (Materials and Environment), experimental error on data measures (END), meta-model (reliability and sensitivity) and reliability analysis, predictive models (chemical degradation), probabilistic update (parameters and predictions), propagation of uncertainty (fields and variables) as well as multi-criteria optimization decisions (monitoring and inspection).”

#### 3.2 Scope of Work

The experiments conducted by LANL and LMA (as well as other French teams) is focused on bench-top measurements using concrete blocks as well as *in situ* inspection of a reinforced concrete wall.

### 3.2.1 Blocks

There are 20 concrete blocks, carbonated at several depths, available for testing. The blocks will be kept in a pool to maintain water saturation until the time of measurement, and thus will be fully saturated (with water) at the time of the experiments. The blocks were carbonated only on one side. See Table 1 for details.

Table 1: Concrete block distribution.

Concrete type	C1 (G8 Senso)			
Carbonation depth (mm)	0	10	20	40
Marking	C1-1-x-y	C1-2-x-y	C1-3-x-y	C1-4-x-y
Number of block per team(*)	2	1	1	1
Total number of blocks	8	4	4	4

Blocks are marked as follows: C1-1-x-y

- 1, 2, 3 or 4 : expected carbonation depth (1 : 0 ; 2 : 10 ; 3 : 20 ; 4 : 40 mm)
- x : number (from 1 to 8 or from 1 to 4)
- y : Letter associated with a team (T : Toulouse ; N : Nantes ; A : Aix ; B : Bordeaux)

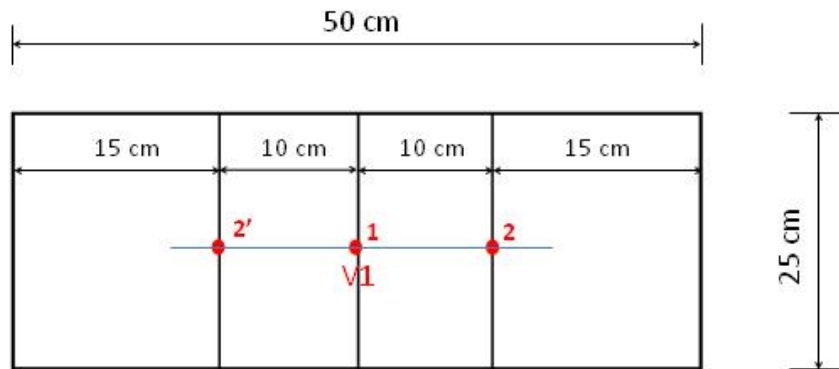


Figure 13: Location of measurement points on concrete blocks.

#### 3.2.1.1 Variability V1

For the blocks C1-1-1-T, C1-2-1-T, C1-3-1-T and C1-4-1-T, we will do a variability test V1 (10 measures at the same point) on the Toulouse blocks. As such, we will have V1 results for the four depths of carbonation on the same samples.

#### 3.2.1.2 Variability V2

For each block, three measurements will be performed 10cm apart as shown on Fig. 13.

Table 2: Summary of measurements to be made on concrete blocks.

Dalle	C1-1-1-T	C1-2-1-T	C1-3-1-T	C1-4-1-T	16 other blocks	Number of measures
V1	10 measurements at point 1	0 measurements	40 measurements			
V2	2 measurements (Pts 2 and 3)	3 measurements (Pts 1, 2, 3)	56 measurements			
TOTAL						96 measurements

96 total measurements will be performed on the blocks.

### 3.2.2 Wall

The wall of C1 concrete (Fig. 14) in ambient thermal and hygrometry conditions, is composed of three parallel stripes, each with a different carbonation depth. Measurements will be done on both sides of the wall, one side having rebar, the other not. Figure 15 shows the zones and points of measurement. As a reminder, the wall has three depths of carbonation 0, 20 and 40 mm, shown by 3 vertical stripes. By analogy with the blocks, we note 1 for 0 mm depth, 3 for 20 mm and 4 for 40 mm. The face with rebar is denoted using the letter f so 1f, 3f, and 4f. Measurements will be done at the center of the rebar mesh, which gives 4 rows 20 cm apart for each carbonation depth. Those rows are denoted A, B, C, D from top to bottom.

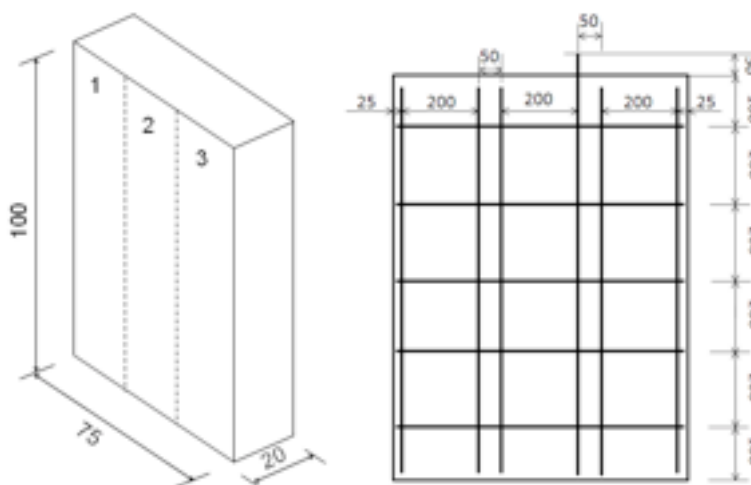


Figure 14: Concrete wall with carbonation zones identified.

#### 3.2.2.1 Variability V1

Ten measurements will be performed at each selected point. Points selected for measurement are 3C (side without rebar) and 3fC (side with rebar).

**3.2.2.2 Variability V1a**

The goal is to analyze the spreading of the results within the region investigated by one measure. We propose to do 10 measurements within the region investigated. For example, if we consider that the measurement at one point affects a zone of 10cm, we will take one measurement every centimeter around point 3 (10cm on each side, so a total of 21 measurements).

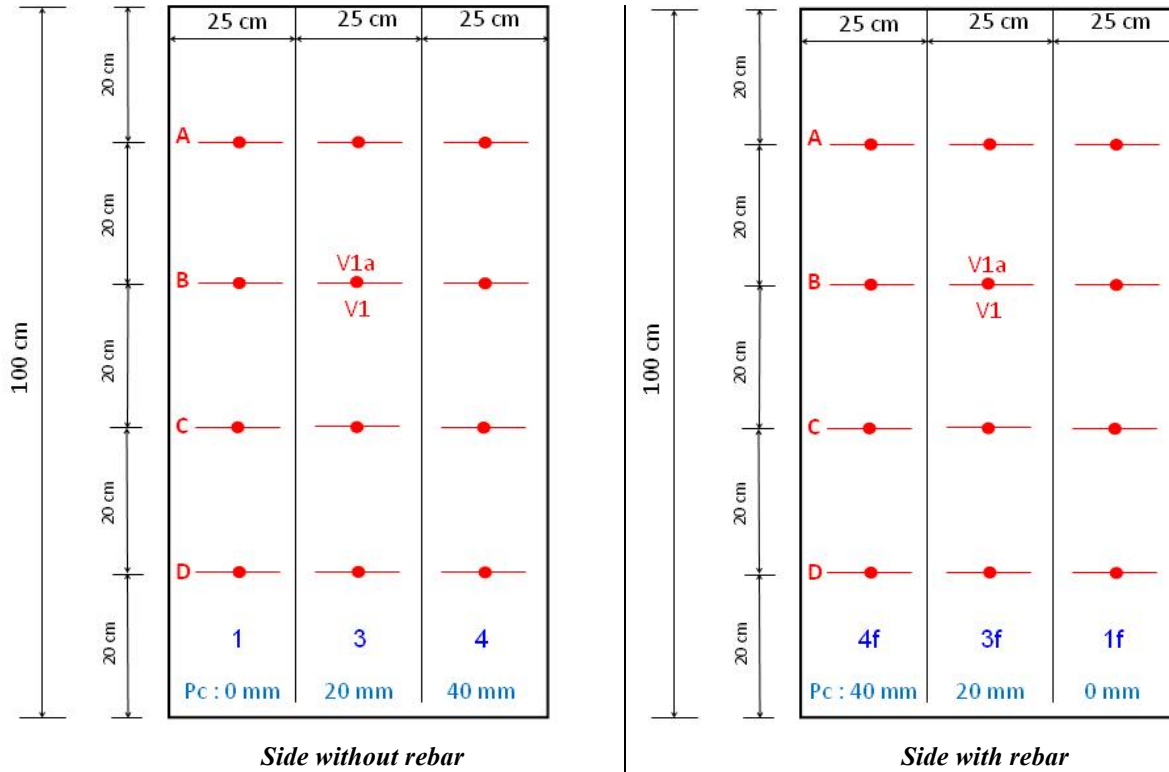


Figure 15: Location of measurement points on the concrete wall.

**Table 3: Summary of measurements to be made on concrete wall.**

	<b>Side without rebar</b>	<b>Rebar side</b>	<b>Number of measurements</b>
<b>V1 in 3C and 3fC</b>	10 measurements in 3C	10 measurements in 3fC	<b>20 measures</b>
<b>V1a in 3C and 3fC</b>	Number of measurements depends on technique (20 for GPR)	Number of measurements depends on technique (20 for GPR)	<b>Depends on techniques</b> 40 for GPR
<b>Other Points</b>	11 measurements	11 measurements	<b>22 measurements</b>
<b>TOTAL</b>			<b>42 + V1a</b> 82 measurements for GPR

*82 total measurements will be performed on the wall.*

### **3.3 EvaDéOs Results**

Testing is currently ongoing. Results from the LANL/LMA collaborative portion of the EvaDéOs project will be reported upon completion. Other portions of the EvaDéOs project will be reported providing release from ANR.

### **3.4 Additional Concrete Studies**

Bench-top concrete studies are also planned for summer 2013 at LANL using the nondestructive techniques RUS, NRUS, TREND and DAE on thermally damaged samples, culminating in destructive compressive testing. This testing will allow for a relationship between nonlinear elasticity parameters and ultimate strength.

Facility scale inspection is planned to take place at LANL’s Los Alamos Neutron Science Center (LANSCE) facility (decommissioned Area-A) where radiation damaged concrete is available in the concrete pads beneath the old beam targets. Both onsite inspection (using TREND) of the concrete pad and laboratory testing of extracted core samples (RUS and NRUS) will be conducted. Current status of this effort is awaiting a GPR survey by LANSCE staff in order to define regions where core samples can be extracted. A radiation survey has been completed, which defined 3 main locations for inspection (0, 5 and 15 mR/hr). Inspection of these regions, and extractions of core samples, will be conducted once all permissions have been obtained.

A future study relating nonlinear elastic wave spectroscopy and related techniques to microstructural features associated with various damage mechanisms in concrete is scheduled to be conducted with the EMPA/ETH-Zurich concrete characterization lab. EMPA’s Michele Griffa will provide damaged samples of concrete due to various AAR mechanisms for nonlinear ultrasonic testing. Microstructural inspection and characterization will also be conducted at EMPA. Drs. TJ Ulrich (LANL) and Cedric Payan (LMA) have been invited to collaborate on this effort.

## 4. References

- [1] Y. Ohara, H. Endo, T. Mihara, K. Yamanaka, “Ultrasonic Measurement of Closed Stress Corrosion Crack Depth”, *Japanese Journal of Applied Physics*, 48 (2009) 07GD01-1-6.
- [2] Y. Ohara, T. Mihara, R. Sasaki, T. Ogata, S. Yamamoto, Y. Kishimoto, K. Yamanaka, “Imaging of Closed Cracks Using Nonlinear Response of Elastic Waves at Subharmonic Frequency”, *Applied Physics Letters*, 90 (2007) 011902-1-3.
- [3] Y. Ohara, S. Yamamoto, T. Mihara, K. Yamanaka, “Ultrasonic Evaluation of Closed Cracks Using Subharmonic Phased Array”, *Japanese Journal of Applied Physics*, 47 (2008) 3908-3915.
- [4] K. V. D. Abeele, “Multi-Mode Nonlinear Resonance Ultrasound Spectroscopy for Defect Imaging: An Analytical Approach for the one-dimensional case”, *Journal of the Acoustical Society of America*, 122 (2007) 73-90.
- [5] I. Solodov, J. Wackerl, K. Pfeleiderer, G. Busse, “Nonlinear Self-Modulation and Subharmonic Acoustic Spectroscopy for Damage Detection and Location”, *Applied Physics Letters*, 84 (2004) 5386-5388.
- [6] EvaDeOS project summary page (in French), <http://i2m.u-bordeaux.fr/departements/genie-civil-et-environnemental-gce/projetsactions/evadeos.html>.

## APPENDIX A

# IMAGING CRACK ORIENTATION USING THE TIME REVERSED ELASTIC NONLINEARITY DIAGNOSTIC WITH THREE COMPONENT TIME REVERSAL

**BRIAN E. ANDERSON\*, T. J. ULRICH, AND PIERRE-YVES LE BAS**

\* Corresponding author's address: Geophysics Group (EES-17), Los Alamos National Laboratory, Los Alamos, NM 87545, bea@lanl.gov

**Proceedings Paper Prepared for the 2013 Spring  
Meeting of the Acoustical Society of America,  
Montreal Canada**

**Abstract:** The time reversed elastic nonlinearity diagnostic (TREND) is a method to allow one to nondestructively evaluate a sample by locating nonlinear scatterers. In the TREND method one creates a localized focus of energy using time reversal at each point of interest. The localized nature of the focus, which is at a higher energy level relative to the wave field nearby thereby amplifying the potential nonlinear signature of the focal location, allows one to image localized nonlinearities. It has also been shown that a focus of energy may be individually created in each of the three independent vector components of vibration using time reversal. Here we show that the use of TREND scans in each of the three vector component directions allows imaging of a crack's orientation. This work is conducted on steel samples, each with cracks at known orientations that were created in a controlled manner. The scaling subtraction method is also used at each scan point to classify the nonlinearity. [This work was supported by the U.S. Dept. of Energy, Fuel Cycle R&D, Used Fuel Disposition (Storage) campaign]

## 1. Introduction

The time reversed elastic nonlinearity diagnostic (TREND) is a time reversal (TR) technique that allows one to focus elastic energy to a particular evaluation point on a sample to inspect that point's nonlinear behavior.<sup>1</sup> Since TR provides a sharp focusing of energy to a particular point in space,<sup>2-3</sup> and therefore at a higher amplitude than the surrounding area, we can assume that any nonlinearity signatures found in the focal signal recorded at the focal point in space pertain mainly to the local region surrounding the focal point.

In a typical implementation of TREND one might bond,  $N$ , piezoelectric transducers to the sample under test and utilize a laser vibrometer to inspect the sample. First a source signal (that one desires to approximately recreate as a focal signal),  $S$ , is emitted from a single piezoelectric transducer (numbered as transducer number  $i$ ). The laser vibrometer then records the *forward* vibration response of the sample at a point of interest,  $R_i(x,y,t)$ . This is repeated for each of the  $N$  transducers. The forward signals are then reversed in time  $R_i(x,y,t) \rightarrow R_i(x,y,-t)$  and the reversed signals are then simultaneously emitted from the respective transducers from which they were originally emitted. If there is a sufficient degree of scattering of energy within the sample then each of the so called *backward*  $R_i(x,y,-t)$  signals independently produces a focus of energy at the laser vibrometer position and they coherently add together. One can then use any one of several techniques to detect nonlinear signatures (e.g. looking for harmonic frequencies or sum and difference frequencies). This entire process (forward and backward emissions) is then repeated at each point of interest on a sample's surface. Signatures of nonlinearity at specific locations can indicate locations of cracking or disbonding.<sup>4</sup>

Ulrich *et al.* showed that one may utilize an out of plane laser vibrometer to focus energy mostly in the out of plane direction on a sample surface or similarly utilize an in plane laser vibrometer to focus energy mostly in the in plane direction on a sample surface (with the direction of the in plane motion pertaining to the orientation of the in plane laser light).<sup>5</sup> With the ability to focus energy in 3 orthogonal directions (the out of plane direction, and two orthogonal in plane directions) at a single point on a sample surface, one can naturally utilize the TREND technique to inspect the nonlinear signatures of that point in three directions. Preliminary experiments to utilize 3D TREND (described above in this paragraph) to image the orientation of cracks and disbonding has been presented previously.<sup>6</sup> Here we present some further experiments, conducted on steel samples with cracks at known orientations, to demonstrate that the orientation of a crack may be imaged using 3D TREND. We utilize the scaling subtraction method (SSM)<sup>7</sup> to classify the nonlinear signature at each evaluation point.

## 2. Experiment Setup

Figure 1(a) displays a photograph of the steel samples used in this study. One sample does not have a crack and is used as a control sample (on the left in the photo). The angles of the crack orientations are at  $77^\circ$ ,  $59^\circ$ ,  $57^\circ$ , and  $29^\circ$  relative to the sample's top surface (the x-y plane) for the samples from left to right as pictured (after the uncracked sample).

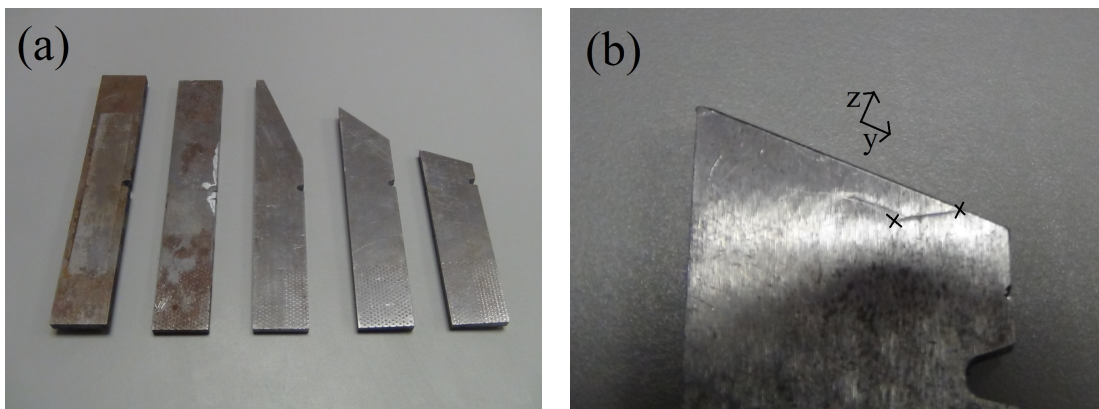


**FIGURE 1.** (a) Photograph of the 5 samples used in this study. (b) Photograph of one of the samples denoting the x, y, and z directions. The crack tips and ends are denoted in the photo.

Eight piezoelectric transducers were bonded (using epoxy) onto a vise that was then used to hold each sample under test. A TREND scan was then conducted with an out of plane laser vibrometer, and two scans with an in plane

laser vibrometer at two orthogonal directions. We define the x, y, and z directions as shown in Fig. 1(b). Note the orientation of the crack on this 29° cracked sample as identified by the marks at the tip and the end of each sample.

A sampling frequency of 10 MHz and a time window of 32768 points (or 3.2768 ms in time) were used in the experiments. The source signal was a sinusoidal pulse of center frequency 75 kHz with a pulse length of 100 μs centered in the 32768 point window was used. For every recording made, 488 averages were done to improve the quality of each recording.

For each of the dimensions of the 3D TREND scan, the TREND procedure is repeated at 5 points spaced 1 mm apart in the x direction, and at 41 points spaced 0.25 mm apart in the y direction. The scanning is done with Cartesian positioning stages.

### 3. Results

Scalerandi *et al.* proposed using a SSM residual metric to quantify the nonlinearity in experiments. In their paper they defined this metric,  $\beta$ , as the sum of the squared amplitudes over a selected period of time of the SSM residual signal. The SSM residual signal is found by making two measurements at different amplitudes, multiplying the lower amplitude signal by the constant representing the amplification difference between the two measurements, and then subtracting the high amplitude measurement from the scaled up lower amplitude measurement. Figure 2 displays the SSM results from the 3D TREND for the 29° cracked sample with the residuals from the x, y, and z directions plotted in (a), (b), and (c) respectively. It should be noted that the crack tip starts at (x = 0 mm, y = 7.5 mm) and ends at (x = 4 mm, y = 8.0 mm).

The x direction results show a gradual increase in  $\beta_x$  from approximately y = 3.0 mm up to the crack tip where it peaks. This is likely the result of motion of the crack's knife edge moving significantly in the x direction relative to the other side of the crack, with a focus at the tip producing the largest motion.

The y direction results for  $\beta_y$  should be expected to be fairly small since y motion should not cause the two crack surfaces to have significantly opposing motions. There is apparently some nonlinearity detected at points right at the crack tip.

The z direction results for  $\beta_z$  should be strongest at the crack tip as the two crack surfaces are forced to clap against one another. We see that this is essentially the case in the results.

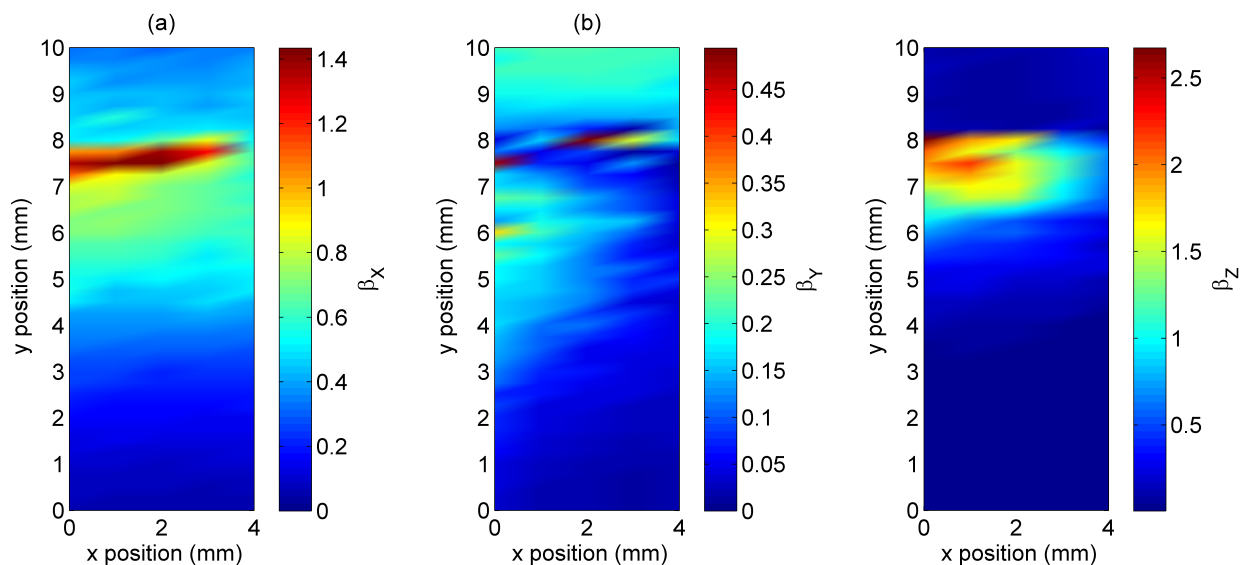


**FIGURE 2.** Spatial maps of the SSM residual,  $\beta$ , from the TREND results with the laser vibrometer setup in different directions for the 29° cracked sample: (a) x direction focusing using the in plane laser, (b) y direction focusing using the in plane laser, and (c) z direction focusing using the out of plane laser. TREND results from (a)-(c) averaged along the x direction for (d) x direction focusing, (e) y direction focusing, and (f) z direction focusing.

## 4. Conclusion

We have shown that 3D TREND, with the use of the SSM technique, can give physical insight into the orientation of a surface bearing crack. Further work will be conducted on the other samples to determine how the orientation of an unknown crack may be determined from similar experiments.

## 5. Acknowledgments

This research was funded by the U.S. Dept. of Energy, Fuel Cycle R&D, Used Fuel Disposition (Storage) campaign.

## 6. References

1. T. J. Ulrich, P. A. Johnson, and A. Sutin, "Imaging nonlinear scatterers applying the time reversal mirror," *J. Acoust. Soc. Am.* **119**(3), 1514-1518 (2006).
2. M. Fink, "Time reversed acoustics," *Phys. Today* **56**, 143-147 (2000).
3. B. E. Anderson, M. Griffa, C. Larmat, T. J. Ulrich, and P. A. Johnson, "Time reversal," *Acoust. Today* **4**(1), 5-16 (2008).
4. T. J. Ulrich, P. A. Johnson, and R. A. Guyer, "Interaction dynamics of elastic waves with a complex nonlinear scatterer through the use of a time reversal mirror," *Phys. Rev. Lett.* **98**(10), 104301 (2007).
5. T. J. Ulrich, K. Van Den Abeele, P.-Y. Le Bas, M. Griffa, B. E. Anderson, and R. A. Guyer, "Three component time reversal: Focusing vector components using a scalar source," *J. Appl. Phys.* **106**(11), 113504 (2009).
6. T. J. Ulrich, P.-Y. Le Bas, R. A. Guyer, B. E. Anderson, M. Griffa, and K. Van Den Abeele, "Three component time reversal imaging using nonlinear elasticity," *J. Acoust. Soc. Am.* **125**(4), Abstract 2635 (2009).
7. M. Scalerandi, A. S. Gliozzi, C. L. E. Bruno, D. Masera, and P. Bocca, "A scaling method to enhance detection of a nonlinear elastic response," *Appl. Phys. Lett.* **92**(10), 101912 (2008).

## **APPENDIX B**

# **DYNAMIC ACOUSTO-ELASTICITY IN A CLOSED FATIGUE CRACKED SAMPLE**

**J. RIVIERE<sup>1</sup>, T. J. ULRICH<sup>1</sup>, Y. OHARA<sup>2</sup>, S. HAUPERT<sup>3</sup>, B.E.  
ANDERSON<sup>1</sup>, AND P.A. JOHNSON<sup>1</sup>**

<sup>1</sup> Los Alamos National Laboratory, Earth and Environmental Sciences, Geophysics Group MS D446, Los Alamos, NM 87545, USA

<sup>2</sup> Yamanaka Laboratory, Dept. of Materials Processing, Graduate School of Engineering, Tohoku University, 02 Aoba Aramaki Sendai 980-8579, Japan

<sup>3</sup> Laboratoire d'Imagerie Parametrique, University of Paris VI, Paris, France.

## **Manuscript In Preparation for Peer Review**

The following manuscript is a draft in preparation for peer-review. Additional finite element modeling (FEM) results and crack mechanics interpretation are underway. The manuscript will be submitted upon inclusion of this additional material.

# Dynamic Acousto-Elasticity in a closed fatigue cracked sample

J. Rivière,<sup>1</sup> T.J. Ulrich,<sup>1</sup> Y. Ohara,<sup>2</sup> S. Hauptert,<sup>3</sup> B.E. Anderson,<sup>1</sup> and P.A. Johnson<sup>1</sup>

<sup>1</sup>*Los Alamos National Laboratory, Earth and Environmental Sciences, Geophysics Group MS D446, Los Alamos, New Mexico 87545, USA.*

<sup>2</sup>*Yamanaka Laboratory, Department of Materials Processing, Graduate School of Engineering, Tohoku University, 02 Aoba Aramaki Sendai 980-8579, Japan.*

<sup>3</sup>*Laboratoire d'Imagerie Parametrique, University of Paris VI, Paris, France.*

(Dated: 15 April, 2013)

Standard nonlinear ultrasonic methods such as wave frequency mixing or resonance based measurements allow one to extract average, bulk variations of modulus and attenuation versus strain level. In contrast, dynamic acousto-elasticity (DAE) provides the elastic behavior over the entire dynamic cycle including hysteresis and memory effects, detailing the full nonlinear behavior under tension and compression. Where prior studies have employed DAE in volumetrically nonlinear materials (e.g., rocks, bone with distributed micro-crack networks) this paper reports on the application to a single localized nonlinear feature, i.e., a fatigue crack, to explore the nonlinear response in regions of the crack length, tip, and undamaged portions of the aluminum sample. As expected linear wave speed is not observed to change in and around the crack, while the linear attenuation and third order elastic moduli (i.e., nonlinear parameters) each indicate a sensitivity to the presence of the crack, though in unique manners. The localized nature of the DAE measurement and its potential for quantifying all of the third order elastic constants makes it a promising technique for both detecting cracks, as well as providing quantitative information on the interaction between cracks and elastic waves, potentially relating these third order moduli to material integrity through this physical understanding.

## I. INTRODUCTION

Probing elastic nonlinearity of materials has broad application including medical imaging, engineering and geophysics, as elastic nonlinearity is a sensitive measure of mechanical damage in solids at many scales. Standard nonlinear ultrasonic methods such as frequency mixing or resonance based measurements provide the means to extract average variations of modulus and attenuation versus strain level. In contrast, the Dynamic Acousto-Elastic (DAE) technique probes the nonlinear elastic response in a localized region. DAE, thus, provides a complementary method for local inspection of material integrity when compared to bulk nonlinear techniques.

In standard (*i.e.*, static) acousto-elasticity, ultrasonic or acoustic waves propagate through the specimen while it is statically stressed at different amplitudes (uniaxial or hydrostatic stress) (1). For isotropic materials, the speed of sound change with stress levels allows one to extract nonlinear parameters A, B, C, *i.e.*, the third order elastic constants (2). The applied stress is usually only compressive for practical reasons and static strain levels have to be relatively high to be measured properly ( $> 10^{-4}$ ).

DAE employs a low frequency wave source instead of a static device to stress the rod shaped sample at its fundamental compressional mode. Strain levels are therefore smaller ( $10^{-8}$  -  $10^{-5}$ ), and the sample is tested under both compression and tension allowing one to obtain the elastic response over a complete dynamic stress cycle. Previous DAE results (3; 4; 5) have shown very complex elastic nonlinearity signatures, in particular hysteretic behaviors and strong effects of material *conditioning* (6; 7).

DAE falls under the broad category of *pump-probe*

methods that have existed in nonlinear acoustics from at least the 1950's (8; 9; 10; 11). It involves application of two dynamic fields, one to perturb the material elasticity (the *pump*) and one to measure the induced elastic changes (the *probe*). DAE uses a low frequency *pump* (LF field) and the *probe* is high frequency pulse (HF field).

Our intent is to explore DAE techniques to characterize localized damage in industrial materials. An aluminum sample containing a single closed fatigue crack is investigated and linear and nonlinear parameters are compared with respect to the crack features.

## II. MATERIALS AND METHODS

### A. Experimental System

The sample shown in Fig. 1a is an aluminium sample ( $L_x = 170$  mm,  $l_y = 30$  mm,  $l_z = 40$  mm) that stands upright on a low frequency compressional source, a piezoceramic disk. The sample has a notch at mid-length ( $x = L_x/2$ ) and a fatigue crack in the plane normal to x-axis. The notch is approximately 3.5 mm-deep, the fatigue crack is 16.5 mm-long on the edges and few millimeters longer on the sample center. The crack, therefore, penetrates to a depth of approximately half the sample width ( $l_z/2 = 3.5 + 16.5$  mm, see schematic in Fig. 2). A high frequency compressional source and associated receiver straddle the sample on each side of the crack, propagating a longitudinal wave along the y-axis. The essential idea is to have a high frequency broadcast, from ultrasonic source to ultrasonic receiver, to probe the elastic state that is modulated in the sample by the low frequency source. Ultrasonic gel is used to ensure good coupling be-

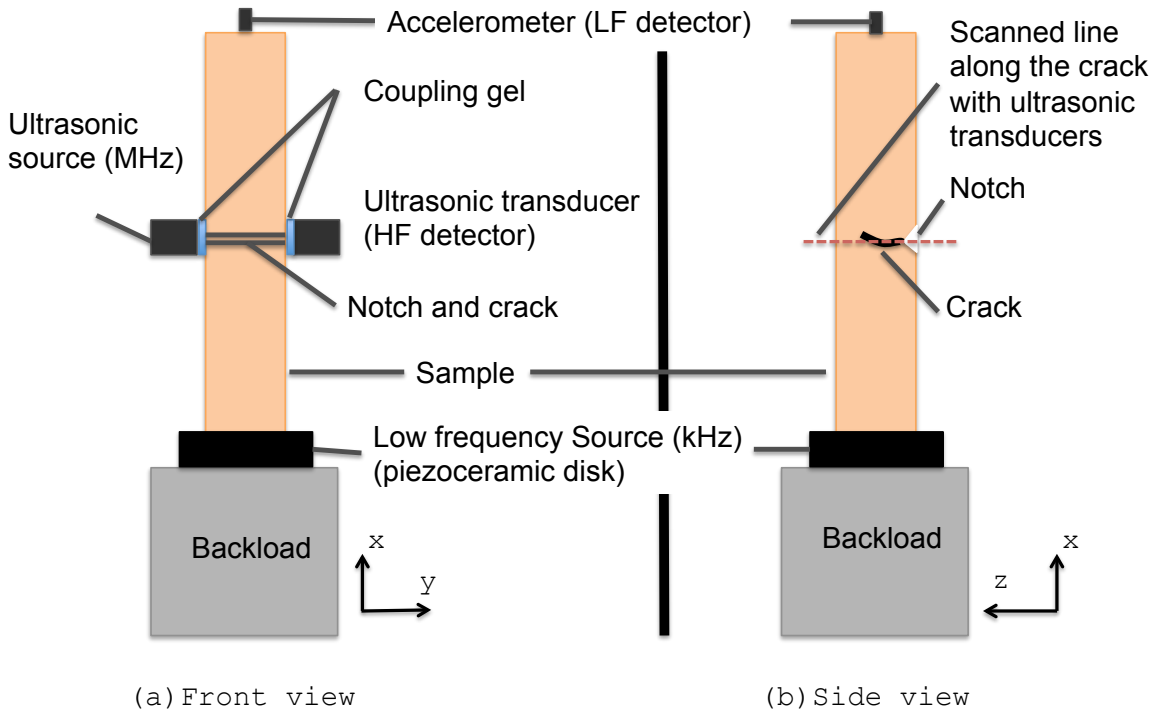


FIG. 1. DAE setup. **(a)** Front view. The low frequency source resonates the sample on its first compressional mode ( $\simeq 7000$  Hz), with fixed-free boundary conditions. Ultrasound pulses at 2 MHz are launched in the sample simultaneously to probe the sample at a given strain level imposed by the low frequency field. An accelerometer placed on the top of the sample allows to measure the low frequency field whereas a second ultrasonic transducer detects the high frequency pulses. The two ultrasonic transducers are placed on each side of the crack so that the longitudinal ultrasonic wave propagates along the crack. **(b)** Side view. The two ultrasonic transducers are moved along the red dashed line to scan the entire sample width.

tween the sample and the transducers. We also put a thin layer of adhesive tape on the sample to prevent the gel to enter the crack. Typically the low frequency  $f_{LF}$  is the frequency of the lowest compressional resonant mode of the cylinder,  $f_{LF} = c/(4L)$  with fixed-free boundary conditions (wavelength  $\lambda = 4L$ ) and where  $c$  is the nominal compressional sound speed in the sample ( $\sim 4800$  m/s, that is  $f_{LF} \simeq 7000$  Hz). Different conditions are required to ensure reliable DAE measurements, see (3; 4; 5) for more details. The high frequency source at 2 MHz is a pulse of duration  $1.5 \mu\text{s}$  *i.e.*, three high frequency periods. The low frequency broadcast/detection and the high frequency broadcast/detection are controlled by a central clock. Both detections are sampled at 50 MHz.

Each pulse propagating during the steady-state is compared with the pulses that traverse the sample before activation of the low frequency source by employing cross-correlation. This allows the determination of  $\tau(t_j)$ , the shift in the time of flight of the high frequency pulse as it crosses the sample at time  $t_j$  (12; 13). Time of flight modulations can be converted into a relative velocity change using:

$$\frac{\Delta c}{c}(t_j) = -\frac{\tau(t_j)}{t_{US}^0} \quad (1)$$

where  $t_{US}^0$  is the time of flight of the reference pulse.

The Fourier transform of each pulse is also performed to evaluate the change in amplitude during the low frequency vibration. The change in attenuation is evaluated using (4):

$$\alpha(t_j) - \alpha_0 = -\ln\left(\frac{A(t_j)}{A_0}\right)/l_y \quad (2)$$

where  $A_0$  is the maximum amplitude of the Fourier transform for the reference pulse, while  $A$  is the maximum amplitude of the Fourier transform for each following pulse.

Finally, changes in the relative sound speed and in attenuation are associated with the strain field  $\epsilon_x(L_x/2, t_j)$ , at the moment of the high frequency broadcast, *i.e.*,  $\frac{\Delta c}{c}(t_j) \Leftrightarrow \epsilon_x(L_x/2, t_j)$  and  $\alpha(t_j) - \alpha_0 \Leftrightarrow \epsilon_x(L_x/2, t_j)$ .

### III. RESULTS

#### A. Linear results (velocity and attenuation)

In Fig. 2, we present the linear results, *i.e.*, velocity and attenuation, obtained along the sample width (red dashed line in Fig. 1). Those results are obtained using

only the two ultrasonic transducers, *i.e.*, without applying the low frequency resonance. We observe no change in velocity as a function of the position, whereas attenuation is much higher (pulse amplitude is much lower) when the wave propagates along the crack. We clearly see an increase in amplitude when moving the US transducers from  $z = 20$  to  $z = 25$  mm. This result confirms the crack length of 20 mm on the edges and few millimeters more on the sample center. One has to note that the ultrasonic transducers are 6 mm in diameter and we perform a measurement each 3 mm. Because values found at each point corresponds to an average over the surface area of the transducers, the measurement made at  $z = 23$  mm, for instance, will correspond to a direct wave propagating in a range of roughly 20-26 mm.

## B. Nonlinear results (DAE)

Fig. 3 gives an example of DAE results when the ultrasonic transducers are at  $z = 19$  mm. We observe that when the low frequency strain is positive (Fig. 3a, tension phase of the sample, crack is opened), the ultrasonic velocity is higher than at rest (Fig. 3b) and the attenuation is lower (Fig. 3c), whereas velocity is lower and attenuation is higher than at rest during the compression phase (negative strain).

A parametric version of Fig. 3 is represented in Fig. 4 for 8 different positions along the width, *i.e.*, relative velocity change and attenuation change as a function of low frequency strain. We observe that the nonlinear signatures are similar all along the crack (Fig. 4a-d) but large changes are observed near the crack tip (Fig. 4e-l). Out of the crack ( $31 < z < 40$  mm), a linear behavior is observed, with no change in velocity and attenuation (Fig. 4o-p).

For all positions along the crack and near the crack tip, we observe that the velocity increases during the tension phase *i.e.*, when the crack opens. Interpretation for this result would be that the direct ultrasonic wave that propagates along the crack is less influenced by asperities at the crack interfaces when the latter is opened. On the contrary, velocity decreases during the compression phase, which would mean that asperities at the interface slows down the direct wave. The slope of the curves “relative velocity change vs LF strain” (Fig. 4a-c-e-g-i-k-m-o) are related to the third order elastic constants (parameter  $\beta$ ). This parameter could be of potential interest to detect cracks and crack tips in particular since the slope appears to be higher for  $z = 19$  and 22 mm.

As far as attenuation change is concerned, we observe different behavior along the crack length and at the crack tip. From  $4 < z < 19$  mm, attenuation increases during the compression phase and decreases during the tension phase. This result seems coherent with interpretation given for velocity observations. The decreasing in attenuation during tension would be due to the fact that asperities at both interfaces produce less friction, as opposed to the compression phase that increases attenua-

tion by putting more asperities in contact and increasing loss processes. At the crack tip ( $z \simeq 22$  mm, Fig. 4j), we observe the inverse effect, *i.e.*, attenuation increasing during the tension phase. In this case, opening the crack that is completely and almost perfectly closed at rest could lead to an increasing in loss processes at the interface.

## IV. CONCLUSION

More work (including more samples for statistical purposes) will have to be done to confirm and understand these different features. From a pragmatical point a view (detection and physical characterization of cracks), the DAE tool seems promising as it allows to obtain the complete description of the nonlinear signature. Furthermore, we notice that information obtained from linear (velocity and attenuation) and nonlinear (DAE) measurements gives different and therefore complementary features for crack characterization.

## V. REFERENCES

- <sup>1</sup>K.W. Winkler and L. McGowan. Nonlinear acoustoelastic constants of dry and saturated rocks. *J. Geophys. Res.*, 109, 2004.
- <sup>2</sup>L.D. Landau and E.M. Lifshitz. *Theory of Elasticity, Third Edition (Theoretical Physics, Vol 7)*. Butterworth-Heinemann, 1986.
- <sup>3</sup>G. Renaud, J. Rivière, S. Hauptert, and P. Laugier. Anisotropy of dynamic acoustoelasticity in limestone, influence of conditioning and comparison with nonlinear resonance spectroscopy. *Accepted to J. Acoust. Soc. Am.*, 2012.
- <sup>4</sup>G. Renaud, P.Y. Le Bas, and P.A. Johnson. Revealing highly complex elastic nonlinear (anelastic) behavior of earth materials applying a new probe: Dynamic acoustoelastic testing. *J. Geophys. Res.*, 117(B6):B06202, 2012.
- <sup>5</sup>G. Renaud, J. Rivière, P.Y. Le Bas, and P.A. Johnson. Hysteretic nonlinear elasticity of berea sandstone at low vibrational strain revealed by dynamic acousto-elastic testing. *Geophys. Res. Lett.*, 40, 2013.
- <sup>6</sup>R.A. Guyer and P.A. Johnson. *Nonlinear mesoscopic elasticity: the complex behaviour of rocks, soil, concrete*. Wiley Vch Pub, 2009.
- <sup>7</sup>J.A. TenCate. Slow dynamics of earth materials: An experimental overview. *Pure and Applied Geophysics*, 168(12):2211–2219, 2011.
- <sup>8</sup>U. Ingard and D.C. Pridmore-Brown. Scattering of sound by sound. *J. Acoust. Soc. Am.*, 28(3):367–369, 1956.
- <sup>9</sup>P.J. Westervelt. Scattering of sound by sound. *J. Acoust. Soc. Am.*, 29(8):934–935, 1957.
- <sup>10</sup>F.R. Rollins Jr, L.H. Taylor, and P.H. Todd Jr. Ultrasonic study of three-phonon interactions. ii. experimental results. *Phys. Rev.*, 136(3A):A597, 1964.
- <sup>11</sup>L.H. Taylor and F.R. Rollins Jr. Ultrasonic study of three-phonon interactions. i. theory. *Phys. Rev.*, 136(3A):A591, 1964.
- <sup>12</sup>G. Renaud, S. Callé, and M. Defontaine. Remote dynamic acoustoelastic testing: Elastic and dissipative acoustic nonlinearities measured under hydrostatic tension and compression. *Appl. Phys. Lett.*, 94, 2009.
- <sup>13</sup>G. Renaud, S. Callé, and M. Defontaine. Dynamic acoustoelastic testing of weakly pre-loaded unconsolidated water-saturated glass beads. *J. Acoust. Soc. Am.*, 128:3344, 2010.

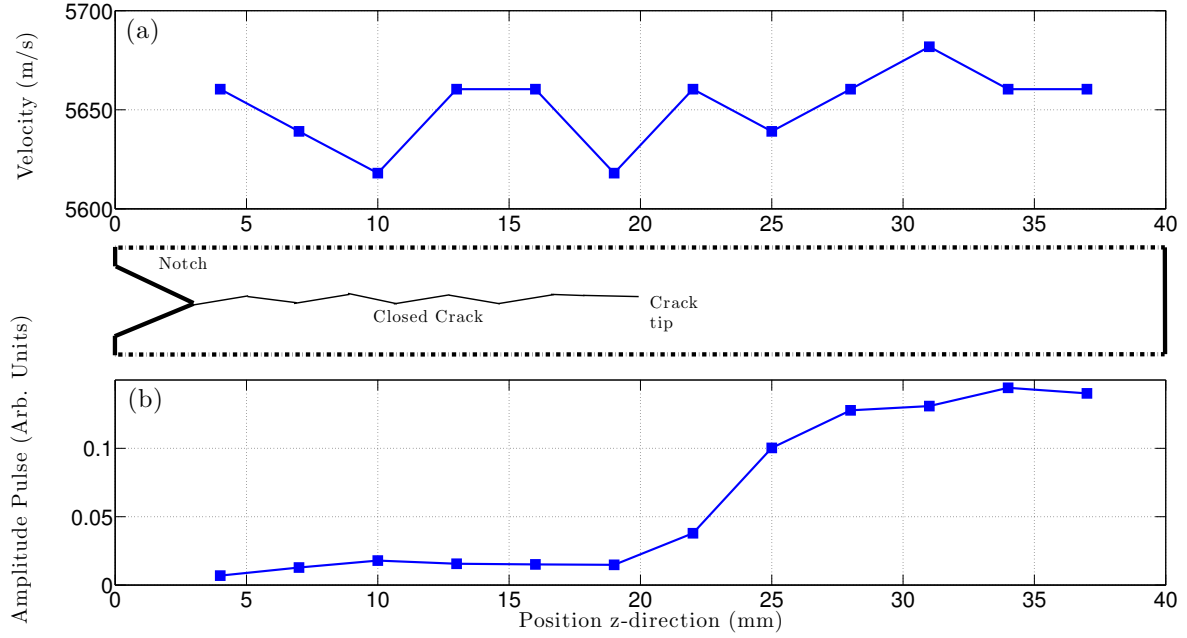


FIG. 2. Linear Results. (a) Velocity as a function of the position along the crack ( $z$ -axis, red dashed line in Fig. 1). No velocity change is observed. (b) Pulse amplitude as a function of the position along the crack ( $z$ -axis). Amplitude is much lower from 0 to 20 mm, where the crack is present, meaning that the wave is much more attenuated when propagating along the crack.

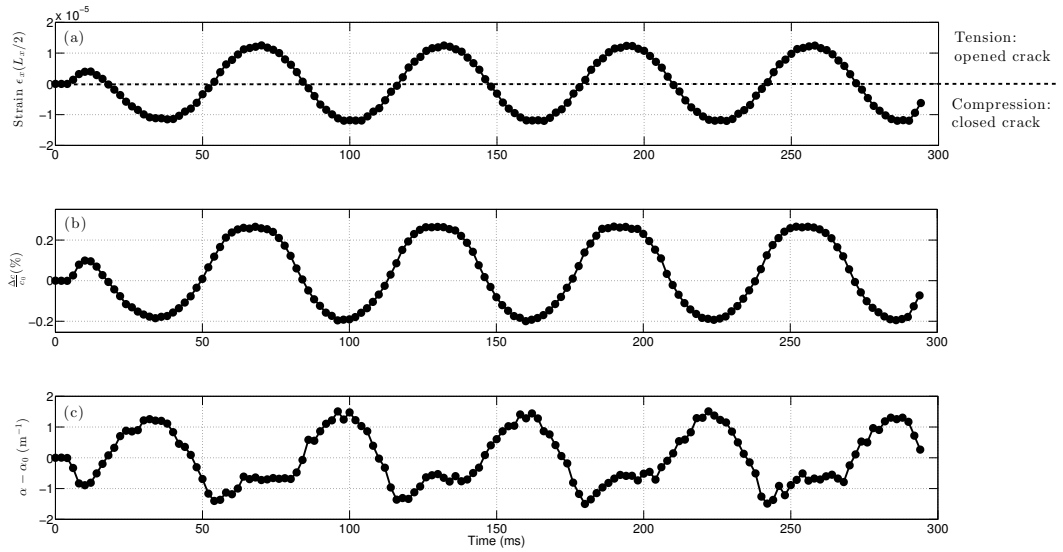


FIG. 3. Example of DAE result for the position  $z = 19$  mm. (a) Strain as a function of time  $t_j$ . Time step of 2 ms corresponds to the time between each ultrasonic pulse broadcast. Positive (respectively negative) strain corresponds to a tension (compression) of the sample. The low frequency source is activated after 5 ms so that first pulses propagate in the medium without being disturbed by the vibration. Extremum absolute strain is about  $1.2 \times 10^{-5}$ , which corresponds to a  $1.4 \mu\text{m}$ -displacement at 7000 Hz. (b) Relative velocity change *versus* time. Velocity is higher in tension phase and lower in compression. (c) Attenuation change *versus* time. Attenuation is higher in the compression phase.

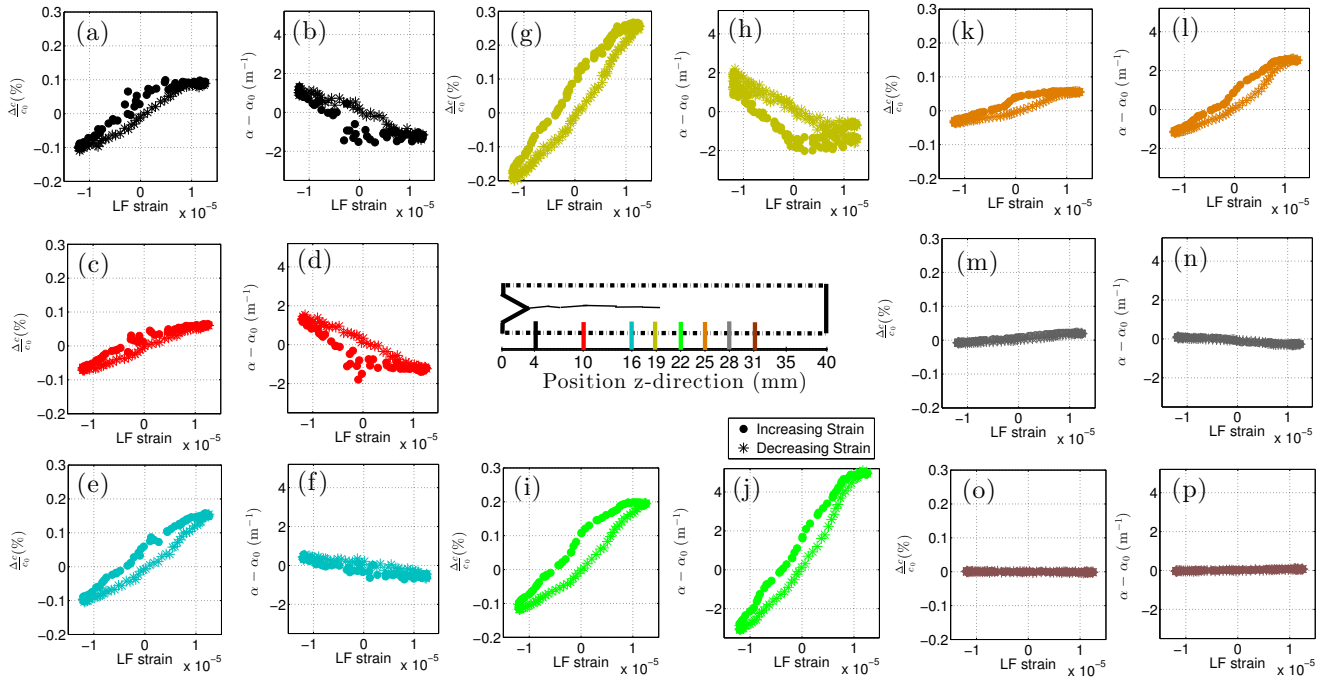


FIG. 4. DAE results for 8 different positions along the sample width  $l_z$ . Relative velocity change  $\frac{\Delta v}{v}$  and attenuation change  $\alpha - \alpha_0$  are represented as a function of low frequency strain  $\epsilon_x$ . Positive (negative) strain corresponds to tension (compression) phase of the sample. Dots and stars correspond to increasing and decreasing strains, respectively. We observe higher nonlinearity for the three positions  $z = 19, 22$  and  $25$  mm, located at the crack tip. The temporal version of (g) and (h) plots are represented in Fig. 3.